



Cite this: RSC Adv., 2017, 7, 16535

Metal/TiO₂ hierarchical nanocomposite arrays for the remarkable enhancement of photocatalytic activity

 Kun Dong,^a Lu Huang,^b Changzheng Wang,^{*a} Ping Xu,^a Yajun Zhang,^a Cuimin Feng,^a Tao Chen,^a Qiang Wang^{*c} and Yang Zhang^{*d}

Metal/TiO₂ hierarchical nanocomposite arrays were assembled by the deposition of aggregated TiO₂ nanoparticles on anodic aluminum oxide templates and the subsequent loading of metal nanoparticles by electrochemical deposition. The as-prepared samples were characterized by X-ray diffraction, scanning electron microscopy, transmission electron microscopy, energy dispersive X-ray spectroscopy and ultraviolet-visible spectroscopy. The photocatalytic activities of the as-synthesized catalysts were evaluated for the degradation of organic dyes. Our experimental results demonstrated that the greatly improved photocatalytic efficiency of the metal/TiO₂ hierarchical nanocomposite arrays resulted from their high surface area and symmetrical arrangement. As a prospective approach for wastewater purification, our work not only enriches the synthetic methodology for TiO₂, but also provides valuable knowledge about nanosized photocatalysts.

Received 9th January 2017

Accepted 3rd March 2017

DOI: 10.1039/c7ra00312a

rsc.li/rsc-advances

1. Introduction

Pioneering works in the early 1970s revealed that hydrogen can be produced by photocatalytic water splitting over a TiO₂ semiconductor under UV irradiation, leading to the broad investigation of nanosized TiO₂ for *in vivo* imaging, cancer therapy, protein separation/purification, dye-sensitized solar cells, perovskite solar cells and bactericides.^{1–11} Utilizing sustainable solar energy is of paramount importance in developing photocatalysts for wastewater treatment. In fact, as a kind of typical azo dyestuff, methyl orange (MO) is one of the main substances in the wastewater industry, and its removal has drawn widespread attention.^{12,13} The effective harvesting of solar energy plays an essential role in developing photocatalysts; other important characteristics include convenient synthesis, scalable production and good stability. Previous works demonstrated that TiO₂-based photocatalysts are potential candidates for the decomposition of organic pollutants in wastewaters.^{14–16} Great efforts have been made to synthesize nanosized TiO₂ with controllable morphology. However,

undoped TiO₂ can be utilized as a UV-light-active photocatalyst due to its wide band gap (~ 3.20 eV).^{17,18} However, the rapid recombination of photo-generated electron-hole pairs results in low degradation efficiency, which extremely limits its photocatalytic applications. There are two potential approaches to solve this problem: synthesizing TiO₂-based nanomaterials with high specific surface areas and preparing TiO₂-based nanocomposites. On one hand, nanosized TiO₂ with a complex structure has improved the photocatalytic activity by increasing the number of surface-active centres. Zhu and co-workers assembled TiO₂ nanoparticles (NPs) with sizes of 4–5 nm into spherical aggregates through the chemical reaction between cyclohexane and cetyltrimethylammonium.¹⁹ Yang and co-workers first reported the preparation methods of hierarchically ordered metal oxide nanomaterials, which significantly broaden the assembly strategies for porous nanomaterials.²⁰ Therefore, TiO₂ NPs can be encapsulated into nanochannels when anodic aluminum oxide (AAO) templates are immersed into the TiO₂ sol solution due to capillary action. The TiO₂ NPs preferably deposit on the wall of the AAO template and then gather in the pore canal.^{21,22} Regardless of the sizes and shapes of the TiO₂ NPs, the controllable synthesis of TiO₂ hierarchical nanoarrays (HNAs) can be achieved by tuning the concentration, immersion time and reaction temperature of the TiO₂ sol.^{23–25} On the other hand, several metal (Ag, Au, and Pt) loading routines have been used to improve the photoresponse of nanosized TiO₂, such as chemical reduction, ion impregnation, impregnation-reduction, photodeposition and electrochemical deposition.^{26–39} In particular, metal ions can be

^aKey Laboratory of Urban Stormwater System and Water Environment, Ministry of Education, Beijing University of Civil Engineering and Architecture, Beijing 100044, PR China. E-mail: changzhwang@163.com; Tel: +86 10 68322131

^bLiupanshui Normal University, Liupanshui 553004, PR China

^cLaboratory of Micro- and Nano-sized Functional Materials, Capital Normal University, Beijing 100048, PR China. E-mail: qwchem@gmail.com; Tel: +86 10 68902523

^dBeijing Institute of Nanoenergy and Nanosystems, Chinese Academy of Sciences, National Center for Nanoscience and Technology (NCNST), Beijing 100083, PR China. E-mail: zhangyang@binn.cas.cn; Tel: +86 10 82854792



dispersed uniformly on the surface of TiO_2 permeated in the gap between TiO_2 aggregates using electrochemical deposition.

In the past decade, extensive efforts have been directed towards the photodegradation of organic pollutants in a highly efficient manner.^{14,40-47} Nevertheless, quite a few studies have reported the photodegradation of organic dyes using TiO_2 photocatalysts with hierarchical nanostructures.⁴⁸⁻⁵¹ In the initial process of photocatalytic degradation, electron-hole pairs are generated under light illumination, separated on the semiconductor surface, and then reacted with organic chemicals in solution.⁵²⁻⁵⁵ During photocatalytic progress, the enhanced performance can generally be ascribed to the increased reactive surface area or reduced recombination of photo-generated electron-hole pairs, which are regarded as different contributors to the photocatalytic efficiency.^{56,57} In principle, the modification of the photocatalyst surface with metal NPs will facilitate charge-carrier transport and reduce charge-carrier recombination.⁵⁸

In this work, we present a novel approach to fabricate metal/ TiO_2 hierarchical nanocomposite arrays (HNCAs), and Ag and Au are selected as representative metals. First, TiO_2 HNAs were assembled *via* the aggregation of TiO_2 NPs with the help of an AAO template. Second, Ag (or Au) was loaded on the TiO_2 HNAs by electrochemical deposition. The synthetic strategy for complex nanostructured TiO_2 provides an impressive pathway for light response through the controllable loading of metal NPs. The as-prepared metal/ TiO_2 HNCA samples were examined for the photocatalytic degradation of MO under UV light illumination. Our experimental results revealed that the photocatalytic efficiency of the metal/ TiO_2 HNCAs was enhanced comparison to the TiO_2 HNAs, suggesting promising prospects for the degradation of organic pollutants.

2. Experimental section

2.1 Materials

All reagents in this work were used as received without further purification. Titanous sulfate $[\text{Ti}(\text{SO}_4)_2]$, hexadecyl trimethyl ammonium bromide ($\text{C}_{19}\text{H}_{42}\text{BrN}$, CTAB), oxalic acid, cyclohexane, ethyl alcohol, acetone, deionized water, concentrated sulfuric acid (H_2SO_4 , 98%) and MO were purchased from Sinopharm Chemical Reagent Beijing Co. Ltd. AAO templates were prepared by the anodization of aluminum plates in oxalic acid solution.

2.2 Preparation of TiO_2 NPs

TiO_2 NPs were prepared by a microemulsion method, and the procedure is briefly described here.²⁵ First, 2.0 g CTAB was dissolved in 100 mL distilled water. Second, 2 mL concentrated H_2SO_4 , 2.5 mL cyclohexane and 1 g $\text{Ti}(\text{SO}_4)_2$ were sequentially added into the CTAB solution, which was then poured into a 250 mL round-bottom flask. After stirring the abovementioned mixture for 1 h, a transparent microemulsion was obtained. Third, a white precipitate was obtained after refluxing for 1 h (at 100 °C). Fourth, the precipitate was centrifuged at a rotation rate of 10 000 rounds per s and rinsed sequentially with

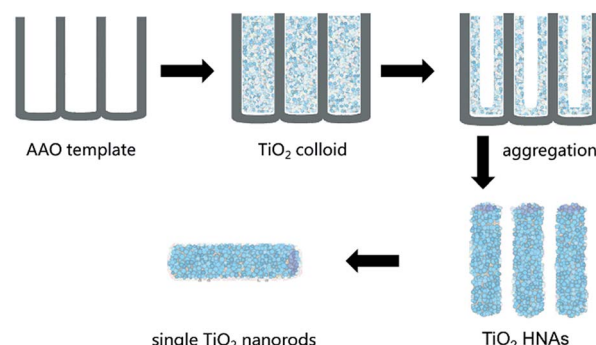
deionized water, ethanol and acetone. To remove unreacted chemicals and other impurities, the washing process was conducted three times. Finally, the product was collected by drying the sediment at 40 °C for 6 h. The as-synthesized sample, which was in the form of a white powder, in agreement with previous reports, was dispersed in ethanol solution.⁵⁹⁻⁶¹

2.3 Preparation of TiO_2 HNAs

As shown in Scheme 1, the assembly of aggregated TiO_2 NPs was carried out according our previous work. A homemade AAO template was fabricated by a two-step anodization process. The AAO template with pore sizes between 80 and 100 nm was employed. Briefly, a gold film was deposited on one side of the AAO template and heated for 5 min to block one side of the through-hole AAO template, which was convenient for the assembly of TiO_2 . The AAO template was then immersed in an ethanol solution of TiO_2 colloids (0.5 mg/100 mL) for 24 h at room temperature. In fact, the deposition of the TiO_2 NPs on the channel walls was driven by electrostatic attraction. The AAO template was finally removed by dissolving it in 6 M NaOH aqueous solution, and the resulting sample was then washed several times with deionized water. Longer lengths and higher specific surface areas of the TiO_2 HNAs can be conveniently obtained by extending the deposition time.

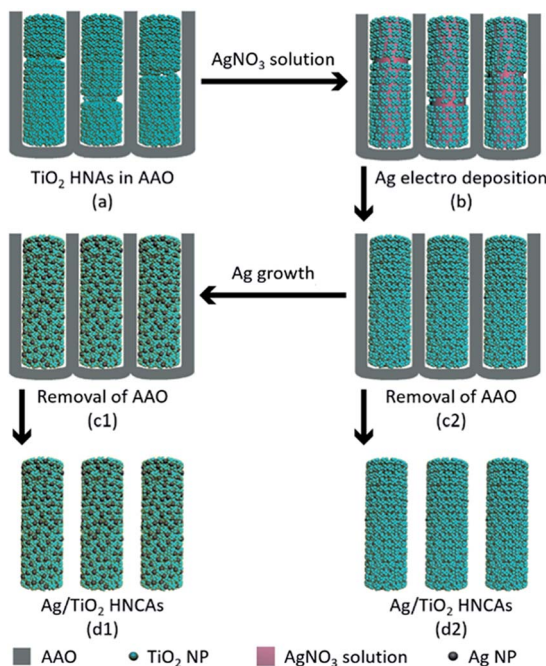
2.4 Preparation of metal/ TiO_2 HNCAs

The aggregated TiO_2 NPs served as the building blocks to assemble TiO_2 HNAs and metal/ TiO_2 HNCAs. The Ag/ TiO_2 HNCAs were synthesized by facile electrochemical deposition method. In a three-electrode system, the TiO_2 HNAs was used as the working electrode, Ag/AgCl as the reference electrode and the Pt wire as the counter electrode. The system was immersed in an AgNO_3 aqueous solution with a voltage of -0.6 V, and the deposition time was set to 20 min. After polishing the redundant TiO_2 NPs, dissolving the AAO template with 6 M NaOH and washing with deionized water, the synthesis of Ag/ TiO_2 HNCAs was achieved (Scheme 2). For the synthesis of Au/ TiO_2 HNCAs, the electrolyte was switched to HAuCl_4 , and the deposition potential was set to -0.4 V accordingly.



Scheme 1 Schematic illustration of the assembly of TiO_2 HNAs in AAO channels.





Scheme 2 Schematic illustration of the preparation process of Ag/TiO₂ HNCAs.

2.5 Characterization

The crystal structures of the as-synthesized samples were characterized by X-ray diffraction (XRD). The morphologies and sizes of the samples were investigated by scanning electron microscopy (SEM, Hitachi S4800) with energy dispersive X-ray spectrometry (EDX) and transmission electron microscopy (TEM, JEOL JEM-2100F). A UV-Vis spectrometer (Hitachi U-3010) was used to study the optical properties of the samples. X-ray photoelectron spectroscopy (XPS) measurements were performed using a Thermo Fisher Scientific USA ESCA Lab250 spectrometer with monochromatic Al K-alpha X-rays, a hemispherical analyzer and a sample stage with multi-axial adjustment to obtain the compositions of the sample surfaces. The UV-Vis diffuse reflectance spectra were obtained using a PerkinElmer Lambda 600S UV/Vis spectrometer equipped with an integrating sphere assembly. The spectra were recorded at room temperature in air from 200 to 800 nm. The photocatalytic properties of the photocatalyst materials were measured using an ultraviolet and visible spectrophotometer (DR6000, HACH).

2.6 Photocatalytic activities

The photocatalytic performances of the aggregated TiO₂ NPs, TiO₂ HNAs, and metal/TiO₂ HNCAs were investigated. For all the photocatalysts, the photocatalytic degradation process was carried out in a 100 mL quartz tube under UV light illumination (UV lamp, 300 W). The temperature was kept at ambient temperature with the assistance of cooling water. A UV-Vis spectrophotometer was used to record the absorption spectra of the MO solutions after the centrifugation of TiO₂. The residual concentrations of the MO solutions were determined by the characteristic absorption peak at 462 nm. To achieve the

optimum photocatalytic conditions of the as-prepared samples, the amount of photocatalyst was varied from 20 to 50 mg L⁻¹. The absorbance of the testing solution was measured for 1 h to evaluate the decomposition rate of MO. At particular time intervals, aliquots were withdrawn from the system, and the TiO₂ NPs were separated from the solution by centrifugation. The residual MO solution was used to characterize the concentration by recording its absorbance intensity.

3. Results and discussion

3.1 Structural and composition analysis

Fig. 1a shows a relatively low-magnification SEM image that reveals the overall morphology of the aggregated TiO₂ NPs. As shown in Fig. 1b, TEM characterization reveals that TiO₂ NPs with diameters ranging from 20 to 30 nm were synthesized. The cationic surfactant CTAB on the surfaces of the TiO₂ NPs effectively restricted particle growth, thus preventing excessive aggregation. Fig. 2 shows the existence of Ti (32.04%) and O (63.15%) elements in the as-prepared sample. The peak of S originates from Ti(SO₄)₂ and concentrated H₂SO₄.

TiO₂ HNAs with mesoporous aggregated NPs can be seen in Fig. 3. As deposition times less than 12 h, aggregated TiO₂ NPs directly assembled into the AAO template and formed nanowire arrays with heights of ~200 nm. Extending the deposition time to 36 h, highly oriented TiO₂ HNAs with longer lengths and larger surface areas can be observed after the removal of the AAO template. The increased surface area of the TiO₂ HNAs may facilitate the photocatalytic degradation of organic pollutants, which will be discussed below.

The XRD patterns of the aggregated TiO₂ NPs and TiO₂ HNAs are presented in Fig. 4. The characteristic diffraction peaks at 25.306°, 37.800°, 48.039°, 55.064°, 62.692°, and 75.055° can be indexed to the crystal planes of (101), (004), (200), (211), (204) and (215), respectively, indicating the formation of anatase TiO₂. The morphologies and sizes of the TiO₂ NPs were characterized by SEM and TEM, respectively. In fact, the TiO₂ HNAs possess high surface areas and large numbers of active centres, which can be utilized to load metals into the interior spaces of the complex nanostructures.

Fig. 5a shows that when the TiO₂ HNAs was immersed in the AgNO₃ (or HAuCl₄) electrolyte solution, the surfaces of TiO₂ HNAs were filled with metal ions. The surfaces of TiO₂ HNAs were decorated with ultrafine Ag NPs after electrochemical

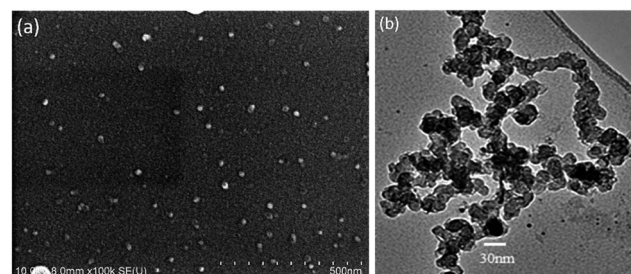
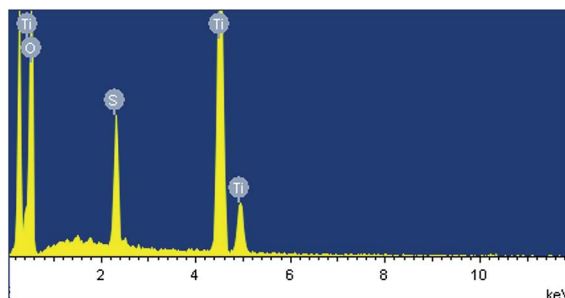
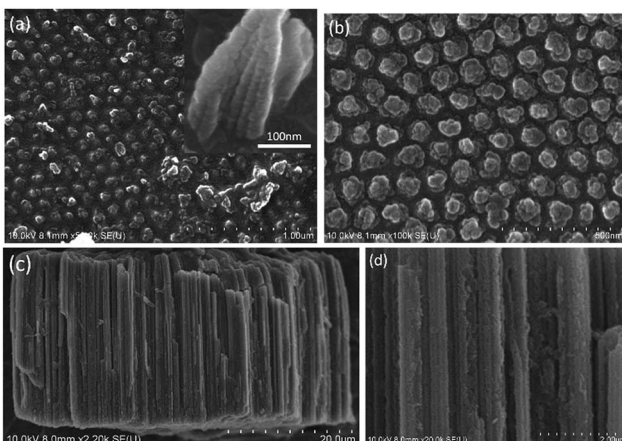
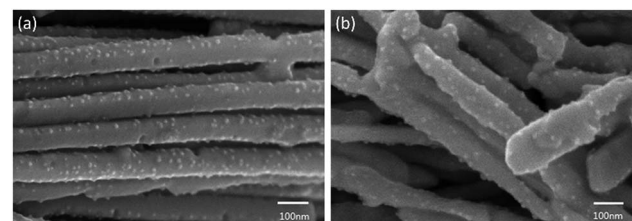
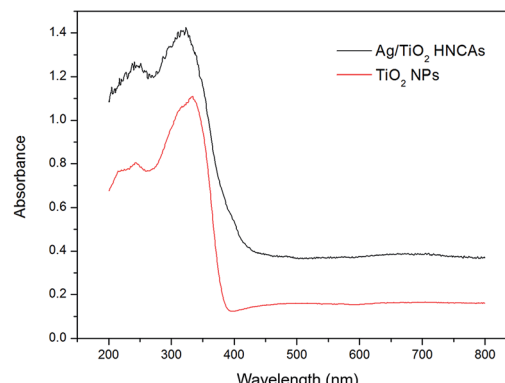


Fig. 1 (a) SEM and (b) TEM images of aggregated TiO₂ NPs.

Fig. 2 EDX image of aggregated TiO_2 NPs.Fig. 3 (a and b) Top and (c and d) cross-sectional images of TiO_2 HNAs.

deposition. The surface roughness seems to decrease upon loading with Ag (or Au), indicating that metal NPs may preferentially deposit in the gaps between aggregated TiO_2 NPs. Compared to TiO_2 HNAs, the lengths of Ag/TiO_2 (or Au/TiO_2) HNCAs are longer, and their continuity is better. Furthermore, other defects are also reduced.

Fig. 6 shows the typical UV-Vis diffuse reflectance spectra of the prepared pure TiO_2 NPs and Ag/TiO_2 HNCAs. In this case, we observed that the pure TiO_2 NPs have no ability to respond under visible light; however, the absorption of the Ag/TiO_2 HNCAs extends significantly into both the ultraviolet and visible regions. It is clear that the incorporation of Ag results in a substantial red shift of the absorption of TiO_2 . According to the results, the observed absorption of the Ag/TiO_2 HNCAs in

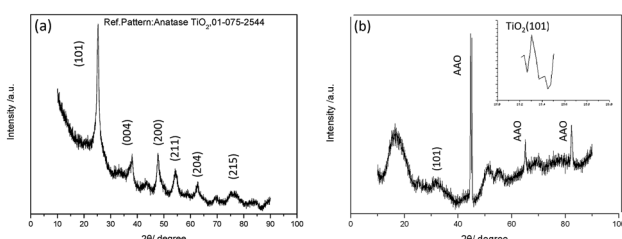
Fig. 5 SEM images of (a) Ag/TiO_2 HNCAs and (b) Au/TiO_2 HNCAs.Fig. 6 UV-Vis diffuse reflectance spectra of the prepared pure TiO_2 NPs and Ag/TiO_2 HNCAs.

the visible-light range can be attributed to the surface plasmon resonance (SPR) absorption of Ag NPs excited by light irradiation over the sample and the restraint of the electron–hole pair recombination. Obviously, the boosted light absorption contributes to enhancing the photoelectronic efficiency and therefore the photocatalytic activity.

The XPS spectra of the Ag/TiO_2 HNCAs present more evidence of Ag NP deposition. The results (Fig. 7a) clearly show three major sets of peaks corresponding to the O 1s, Ti 2p, and Ag 3d states in the Ag/TiO_2 HNCA sample. No trace of any impurities was observed, except for a small amount of adventitious carbon from the XPS instrument itself. From Fig. 7b, it can be seen that the Ag 3d_{5/2} and Ag 3d_{3/2} spin-orbitals are located at binding energies of 367.7 and 373.8 eV, respectively. The 6.1 eV difference between the binding energies of the peaks is also characteristic of metallic Ag 3d states. This binding energy also indicates that Ag mainly exists in the Ag^0 state on the surfaces of the TiO_2 HNAs.

3.2 Photocatalytic activities

The optimum concentration of MO was determined by photocatalytic experiments. Certain amounts of aggregated TiO_2 NPs were dispersed into 500 mL MO solutions with initial concentrations of 20, 30 and 50 mg L⁻¹. As demonstrated in Fig. 8a, the photodegradation of MO (20 and 30 mg L⁻¹) is almost finished within 20 min. By increasing the MO concentration to 50 mg L⁻¹, the degradation rate was reduced to 75%. This can be ascribed to the fact that the photocatalytic reaction principally occurs on the surface of the photocatalyst. For the intermediate

Fig. 4 XRD patterns of the (a) aggregated TiO_2 NPs and (b) TiO_2 HNAs.

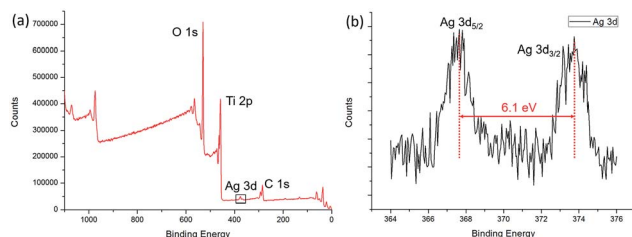


Fig. 7 (a) XPS spectrum of the prepared Ag/TiO₂ HNCAs and (b) high-resolution XPS spectrum of Ag 3d.

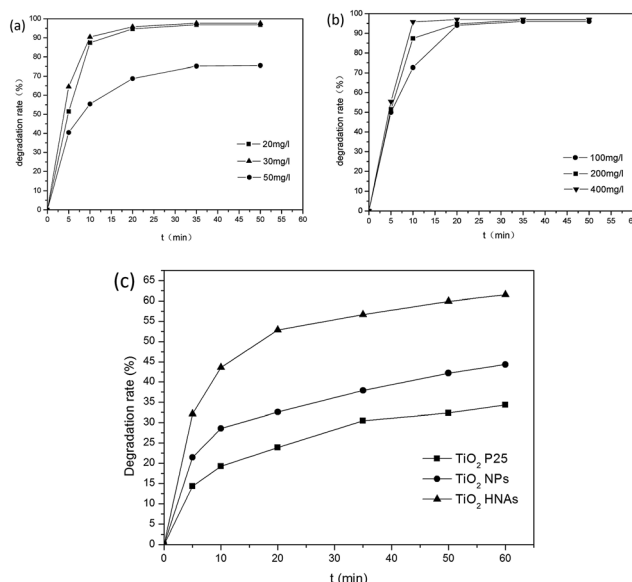


Fig. 8 Effects of the initial concentration of MO, photocatalyst loading amount and light illumination conditions on the photocatalytic activities: (a) initial concentrations of MB are 20, 30 and 50 mg L⁻¹ (100 mg L⁻¹ aggregated TiO₂ NPs as photocatalyst); (b) dosages of aggregated TiO₂ NPs are 100, 200, and 400 mg L⁻¹ (initial MO concentration is 30 mg L⁻¹); (c) degradation of MO in the presence of the aggregated TiO₂ P25, TiO₂ NPs and TiO₂ HNAs after light illumination with a UV lamp (300 W). The concentrations of MO at different time intervals were measured.

concentration of MO, a sufficient amount of ·OH can be applied to promote the photocatalytic reaction in the region of the TiO₂ NP surfaces. Furthermore, we investigated the influence of different dosages of aggregated TiO₂ NPs on the photocatalytic activities. As displayed in Fig. 8b, 95% of MO can be degraded in the presence of TiO₂ NPs after 20 min. However, we found that the performance obtained with 200 mg L⁻¹ photocatalyst was better than that obtained with 100 mg L⁻¹ and close to that obtained with 400 mg L⁻¹ in the first 10 min. To evaluate the photocatalytic efficiency, we compare the degradation rate between TiO₂ P25, aggregated TiO₂ NPs and TiO₂ HNAs based on the abovementioned results (Fig. 8c). Herein, the photocatalytic performance was studied under UV light illumination. The experimental results indicated that only a small fraction of MO is degraded when using TiO₂ P25 and aggregated TiO₂ NPs as the photocatalyst.

Fig. 9 shows the photocatalytic degradation rates of MO on the metal/TiO₂ HNCAs and TiO₂ HNAs. The results show that the metal/TiO₂ HNCAs exhibit higher photocatalytic activity than the TiO₂ HNAs, implying that the metal/TiO₂ HNCAs are expected to possess high photocatalytic activity and potential practical applications in the degradation of the organic contaminants in water.

One of the major bottlenecks in TiO₂-based photocatalysis is insufficient surface-active centres. Therefore, the synthesis of nanosized TiO₂ with large surface area plays a vital role in further improving the photodegradation efficiency. Due to the different formation mechanism, the assembly process of TiO₂ NPs on the AAO template is distinguished from those of other nanomaterials. In this work, aggregated TiO₂ NPs deposited in the holes of the AAO template and then assembled as a uniform nanoarray structure. In fact, the lengths of the TiO₂ HNAs can be controlled by controlling the deposition time.⁶²⁻⁶⁴ It should also be noted that the diameters of the TiO₂ HNAs can be tuned by the pore size of the AAO template, which may be another critical aspect in the development of TiO₂ HNAs.

As illustrated in Scheme 3(a), the TiO₂ HNAs are made from aggregated TiO₂ NPs, which facilitate the adsorption of MO molecules on the surface of nanosized TiO₂ as well as the diffusion of MO into the interior spaces of HNAs. The band gap of TiO₂ between the valence band and the conduction band is 3.2 eV. Triggered by UV light illumination, the photogenerated electrons (e⁻) in the valence band transfer to the conduction band, leaving a photogenerated hole (h⁺) in the valence band. Dissolved oxygen (O₂) adsorbed on the TiO₂ surface can capture electrons (e⁻) from nanosized TiO₂ and then produce superoxide anion free radicals (·O₂⁻), which possess strong oxidizing ability. Meanwhile, holes can react with OH⁻ and H₂O adsorbed on the TiO₂ surface to form hydroxyl radical (·OH).⁶⁵⁻⁶⁷ Due to the strong oxidizing ability of ·OH and ·O₂⁻, no intermediate products in the oxidation reaction process are expected. Under continuous UV light illumination, the separated photogenerated electrons and holes in the valence and conduction bands can be employed to photodegrade MO and other organic dyes into CO₂ and H₂O.⁶⁸⁻⁷⁰

Scheme 3(b) demonstrates the photogenerated charge transfer process between TiO₂ and metal NPs. Previous reports

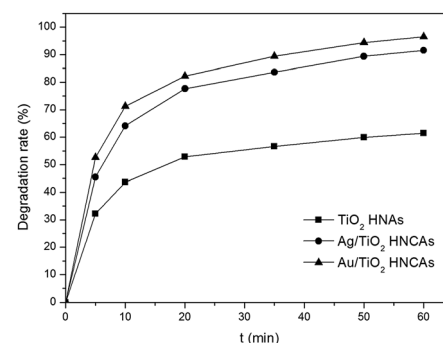
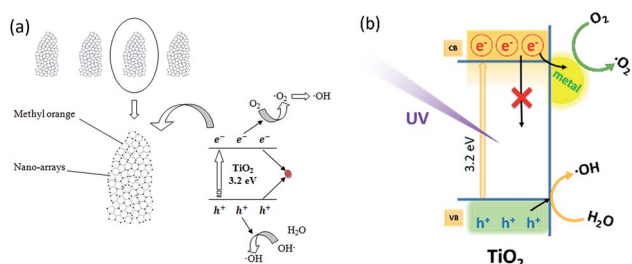


Fig. 9 Photocatalytic degradation rate of MO in the presence of Au/TiO₂ HNCAs, Ag/TiO₂ HNCAs and TiO₂ HNAs after illumination with a UV lamp (300 W).





Scheme 3 Photocatalytic mechanism of the (a) TiO_2 HNAs and (b) metal/ TiO_2 HNCAs.

revealed that the modification of metal NPs on semiconductor surfaces can enhance the photocatalytic efficiency by effectively trapping the photogenerated electrons from metal NPs decorated on the TiO_2 surfaces, or by charge-transfer resulting from the Fermi levels of these metal NPs lower than the conduction bands of the semiconductors.^{71–73} The deposition of metal NPs can be considered as an effective way to suppress electron–hole recombination. Consequently, more holes will be available for the photocatalytic reactions. The promotion is derived from the difference in the electronic work functions between the TiO_2 and deposited metal NPs. Considering the minimum energy value of the conduction band of TiO_2 is still higher than the Fermi energy level of the metal/ TiO_2 composite structure, photogenerated electrons will simultaneously transfer from the TiO_2 to the decorated metal NPs until the equilibrium of the Fermi levels attained under external activation such as UV irradiation. Furthermore, the Schottky barriers formed between metal NPs and TiO_2 can capture the electrons generated at the metal/ TiO_2 HNCA interfaces to prevent electron–hole recombination.^{74–76} The hole in the valence band has a strong oxidation ability, and most of the organic chemicals can be rapidly decomposed into CO_2 , H_2O and other nontoxic substances after UV light illumination. On one hand, electrons have to be triggered to overcome the barrier from TiO_2 to the metal NPs. On the other hand, electrons will be blocked by the barrier. For metal/ TiO_2 HNCAs, the abundant interfacial electrons and photogenerated holes react with O_2 and H_2O molecules under UV irradiation, enhancing the amounts of $\cdot\text{O}_2^-$ and $\cdot\text{OH}$ and improving the photocatalytic activities. Therefore, TiO_2 HNAs can be considered as potential building blocks for chemical sensors and energy-harvesting devices due to their small dimensions, high material quality, large surface-to-volume ratio, *etc.*

4. Conclusions

Using aggregated anatase TiO_2 NPs, we demonstrated a convenient and universal approach to fabricate uniform TiO_2 HNAs with the assistance of an AAO template. Our experimental results revealed that TiO_2 HNAs demonstrate remarkably enhanced photocatalytic activity for the removal of MO compared to aggregated TiO_2 NPs due to its specific large-scale surface characteristics. Metals (Ag and Au) were deposited on the TiO_2 HNA surfaces to form metal/ TiO_2 HNCAs. Compared to the TiO_2 HNAs, the HNCAs exhibit extraordinary photocatalytic

activity for the photodegradation of MO. In this work, we enriched the synthetic methodology for complex nanostructured TiO_2 and provided a strategy to enhance the photocatalytic efficiency. The prepared materials show great potential for the degradation of organic pollutants in wastewaters.

Acknowledgements

This work is financially supported by National Natural Science Foundation of China (NSFC no. 21471103, 51278026, 51678026, 21103008).

Notes and references

- 1 A. Fujishima and K. Honda, *Nature*, 1972, **238**, 37.
- 2 X. Wang, Z. Li, J. Shi and Y. Yu, *Chem. Rev.*, 2014, **114**, 9346.
- 3 J. Schneider, M. Matsuoka, M. Takeuchi, J. Zhang, Y. Horiuchi, M. Anpo and D. W. Bahnemann, *Chem. Rev.*, 2014, **114**, 9919.
- 4 X. Chang, S. S. Thind, M. Tian, M. M. Hossain and A. Chen, *Electrochim. Acta*, 2015, **173**, 728.
- 5 Y. Zhuang, F. Yu and J. Ma, *J. Nanomater.*, 2015, **2015**, 1.
- 6 J. M. Ball, M. M. Lee, A. Hey and H. J. Snaith, *Energy Environ. Sci.*, 2013, **6**, 1739.
- 7 Q. Chen, H. Zhou, Z. Hong, S. Luo, H. S. Duan, H. H. Wang, Y. Liu, G. Li and Y. Yang, *J. Am. Chem. Soc.*, 2014, **136**, 622–625.
- 8 N. J. Jeon, J. H. Noh, Y. C. Kim, W. S. Yang, S. Ryu and S. I. Seok, *Nat. Mater.*, 2014, **13**, 897–903.
- 9 D. Liu and T. L. Kelly, *Nat. Photonics*, 2013, **8**, 133–138.
- 10 M. Liu, M. B. Johnston and H. J. Snaith, *Nature*, 2013, **501**, 395–398.
- 11 M. Ma, Q. Tang, P. Yang and B. He, *RSC Adv.*, 2016, **6**, 82933–82940.
- 12 G. Cappelletti, C. L. Bianchi and S. Ardizzone, *Appl. Catal., B*, 2008, **78**, 193.
- 13 J. M. Meichtry, M. Brusa, G. Mailhot, M. A. Grela and M. I. Litter, *Appl. Catal., B*, 2007, **71**, 101.
- 14 K. Nagaveni, G. Sivalingam, M. S. Hegde and G. Madras, *Appl. Catal., B*, 2004, **48**, 83.
- 15 C. E. Bonançêa, G. M. do Nascimento, M. L. de Souza, M. L. A. Temperini and P. Corio, *Appl. Catal., B*, 2006, **69**, 34.
- 16 D. Li, Y. Guo, C. Hu, C. Jiang and E. Wang, *J. Mol. Catal. A: Chem.*, 2004, **207**, 183.
- 17 M. Dahl, Y. Liu and Y. Yin, *Chem. Rev.*, 2014, **114**, 9853.
- 18 I. J. Puentes-Cárdenas, G. M. Chávez-Camarillo, C. M. Flores-Ortiz, M. D. C. Cristiani-Urbina, A. R. Netzahuatl-Muñoz, J. C. Salcedo-Reyes, A. M. Pedroza-Rodríguez and E. Cristiani-Urbina, *J. Nanomater.*, 2016, **2016**, 1.
- 19 H. Wang, J. J. Miao, J. M. Zhu, H. M. Ma, J. J. Zhu and H. Y. Chen, *Langmuir*, 2004, **20**, 11738.
- 20 P. Yang, T. Deng, D. Zhao, P. Feng, D. Pine, B. F. Chmelka, G. M. Whitesides and G. D. Stucky, *Science*, 1998, **282**, 2244.
- 21 C. C. Wang, C. C. Kei, Y. W. Yu and T. P. Perng, *Nano Lett.*, 2007, **7**, 1566.
- 22 C. Z. Wang, Y. F. E, L. Z. Fan, Z. H. Wang, H. B. Liu, Y. L. Li, S. H. Yang and Y. L. Li, *Adv. Mater.*, 2007, **19**, 3677.



23 J. Q. Li, D. F. Wang, H. Liu, Z. L. He and Z. F. Zhu, *Appl. Surf. Sci.*, 2011, **257**, 5879.

24 J. Yu, Q. Xiang, J. Ran and S. Mann, *CrystEngComm*, 2010, **12**, 872.

25 Y. C. Liang, C. C. Wang, C. C. Kei, Y. C. Hsueh, W. H. Cho and T. P. Perng, *J. Phys. Chem. C*, 2011, **115**, 9498.

26 J. M. Macak, M. Zlamal, J. Krysa and P. Schmuki, *Small*, 2007, **3**, 300.

27 Y. S. Sohn, Y. R. Smith, M. Misra and V. Subramanian, *Appl. Catal., B*, 2008, **84**, 372.

28 L. L. Costa and A. G. S. Prado, *J. Photochem. Photobiol. A*, 2009, **201**, 45.

29 M. J. Zheng, L. D. Zhang, G. H. Li and W. Z. Shen, *Chem. Phys. Lett.*, 2002, **363**, 123–128.

30 X. Zhang, F. Shi, X. Yu, H. Liu, Y. Fu, Z. Wang, L. Jiang and X. Li, *J. Am. Chem. Soc.*, 2004, **126**, 3064–3065.

31 C. L. Yu, Y. Bai, J. C. Chen, W. Q. Zhou, H. B. He, J. C. Yu, L. H. Zhu and S. S. Xue, *Sep. Purif. Technol.*, 2015, **154**, 115–122.

32 S. M. Li, Y. S. Wang, S. Y. Yang, C. H. Liu, K. H. Chang, H. W. Tien, N. T. Wen, C. C. M. Ma and C. C. Hu, *J. Power Sources*, 2013, **225**, 347–355.

33 N. Eliaz, T. M. Sridhar, U. Kamachi Mudali and B. Raj, *Surf. Eng.*, 2013, **21**, 238–242.

34 F. Pishbin, V. Mourino, J. B. Gilchrist, D. W. McComb, S. Kreppel, V. Salih, M. P. Ryan and A. R. Boccaccini, *Acta Biomater.*, 2013, **9**, 7469–7479.

35 C. L. Yu, W. Q. Zhou, H. Liu, Y. Liu and D. D. Dionysiou, *Chem. Eng. J.*, 2016, **287**, 117–129.

36 A. Santibañez, M. Herrera-Trejo, J. Oliva and A. I. Martinez, *Superlattices Microstruct.*, 2016, **100**, 973–982.

37 K. Nagaveni, G. Sivalingam, M. S. Hegde and G. Madras, *Environ. Sci. Technol.*, 2004, **38**, 1600.

38 A. Kumar, L. Rout, L. S. K. Achary, A. Mohanty, R. S. Dhaka and P. Dash, *RSC Adv.*, 2016, **6**, 32074.

39 B. A. Aragaw, C. J. Pan, W. N. Su, H. M. Chen, J. Rick and B. J. Hwang, *Appl. Catal., B*, 2015, **163**, 478.

40 M. Liu, K. L. Lv, G. H. Wang, Z. Y. Wang, Y. X. Zhao and Y. R. Deng, *Chem. Eng. Technol.*, 2010, **33**, 1531.

41 M. Landmann, E. Rauls and W. G. Schmidt, *J. Phys.: Condens. Matter*, 2012, **24**, 195503.

42 M. Lahav, T. Sehayek, A. Vaskevich and I. Rubinstein, *Angew. Chem., Int. Ed. Engl.*, 2003, **42**, 5575.

43 J. Chen, L. Eberlein and C. H. Langford, *J. Photochem. Photobiol. A*, 2002, **148**, 183.

44 M. R. Hoffmann, S. T. Martin, W. Choi and D. W. Bahnemann, *Chem. Rev.*, 1995, **95**, 69.

45 J. C. D’Oliveira, C. Minero, E. Pelizzetti and P. Pichat, *J. Photochem. Photobiol. A*, 1993, **72**, 261.

46 D. Z. Lu, H. M. Wang, X. N. Zhao, K. K. Kondamareddy, J. Q. Ding, C. H. Li and P. F. Fang, *ACS Sustainable Chem. Eng.*, 2017, **5**, 1436.

47 L. J. Li, J. Zhang, J. L. Lei, J. Xu, P. P. Liu, N. B. Li and F. S. Pan, *RSC Adv.*, 2016, **6**, 34507.

48 D. S. Bhatkhande, V. G. Pangarkar and A. A. Beenackers, *J. Chem. Technol. Biotechnol.*, 2001, **77**, 102.

49 G. Sivalingam, K. Nagaveni, M. S. Hegde and G. Madras, *Appl. Catal., B*, 2003, **45**, 23–38.

50 C. L. Yu, K. Yang, Y. Xie, Q. Z. Fan, J. C. Yu, Q. Shua and C. Y. Wang, *Nanoscale*, 2013, **5**, 2142–2151.

51 G. Sivalingam, M. H. Priya and G. Madras, *Appl. Catal., B*, 2004, **51**, 67.

52 S. Liu, J. Yu and M. Jaroniec, *J. Am. Chem. Soc.*, 2010, **132**, 11914.

53 X. Xu, X. Fang, T. Zhai, H. Zeng, B. Liu, X. Hu, Y. Bando and D. Golberg, *Small*, 2011, **7**, 445.

54 S. T. Ong, C. K. Lee, Z. Zainal, P. S. Keng and S. T. Ha, *J. Fundam. Appl. Sci.*, 2009, **5**, 88.

55 L. A. Díaz, W. Solís, P. Peretyagin, A. Fernández, M. Morales, C. Pecharromán, J. S. Moya and R. Torrecillas, *J. Nanomater.*, 2016, **2016**, 1.

56 Y. W. Lin, C. W. Lu, G. P. Yu and J. H. Huang, *J. Nanomater.*, 2016, **2016**, 1.

57 J. Liao, S. Lin, L. Zhang, N. Pan, X. Cao and J. Li, *ACS Appl. Mater. Interfaces*, 2012, **4**, 171.

58 Y. Tang, P. Wee, Y. Lai, X. Wang, D. Gong, P. D. Kanhere, T.-T. Lim, Z. Dong and Z. Chen, *J. Phys. Chem. C*, 2012, **116**, 2772.

59 Y. Kim, H. Joo, N. Her, Y. Yoon, C. H. Lee and J. Yoon, *Chem. Eng. J.*, 2013, **229**, 66.

60 C. L. Yu, F. F. Cao, X. Li, G. Li, Y. Xie, J. C. Yu, Q. Shu, Q. Z. Fan and J. C. Chen, *Chem. Eng. J.*, 2013, **219**, 86–95.

61 T. D. Pham, B. K. Lee and D. Pham Cong, *RSC Adv.*, 2016, **6**, 25346.

62 H. Hossaini, G. Moussavi and M. Farrokhi, *Water Res.*, 2014, **59**, 130.

63 G. Liu, L. Wang, H. G. Yang, H. M. Cheng and G. Q. Lu, *J. Mater. Chem.*, 2010, **20**, 831.

64 W. P. Zhang, X. Y. Xiao, Y. Li, X. Y. Zeng, L. Zheng and C. Wan, *RSC Adv.*, 2016, **6**, 33705.

65 S. Maiti, U. N. Maiti and K. K. Chattopadhyay, *Synth. React. Inorg. Met.-Org. Chem.*, 2014, **44**, 1255.

66 V. Subramanian, E. E. Wolf and P. V. Kamat, *J. Am. Chem. Soc.*, 2004, **126**, 4943.

67 L. L. Lai, W. Wen and J. M. Wu, *RSC Adv.*, 2016, **6**, 25511.

68 M. Amin, J. Tomko, J. J. Naddeo, R. Jimenez, D. M. Bubb, M. Sitener, J. Fitz-Gerald and S. M. O’Malley, *Appl. Surf. Sci.*, 2015, **348**, 30.

69 C. L. Yu, W. Q. Zhou, L. H. Zhu, G. Li, K. Yang and R. C. Jin, *Appl. Catal., B*, 2016, **184**, 1–11.

70 X. Zhang, Y. Zhang, D. Liu, J. Feng, L. Zhou, Y. Yang, X. Guo and X. Li, *RSC Adv.*, 2016, **6**, 34650.

71 S. Banerjee, S. K. Mohapatra, P. P. Das and M. Misra, *Chem. Mater.*, 2008, **20**, 6784.

72 M. Jakob, H. Levanon and P. V. Kamat, *Nano Lett.*, 2003, **3**, 353.

73 C. Liu, R. F. Tong, Z. K. Xu, Q. Kuang, Z. Xie and L. Zheng, *RSC Adv.*, 2016, **6**, 29794.

74 X. He, Y. Cai, H. Zhang and C. Liang, *J. Mater. Chem.*, 2011, **21**, 475.

75 A. L. Linsebigler, G. Lu and J. T. Yates, *Chem. Rev.*, 1995, **95**, 735.

76 A. Wold, *Chem. Mater.*, 1993, **5**, 280.

